JOURNAL OF THE ROYAL SOCIETY Interface

rsif.royalsocietypublishing.org

Research

Cite this article: Ngwenya BT, Magennis M, Podda F, Gromov A. 2014 Self-preservation strategies during bacterial biomineralization with reference to hydrozincite and implications for fossilization of bacteria. *J. R. Soc. Interface* **11**: 20140845.
http://dx.doi.org/10.1098/rsif.2014.0845

Received: 29 July 2014
Accepted: 29 August 2014

Subject Areas:
biogeochemistry, astrobiology, environmental science

Keywords:
biomineralization, fossilization, nucleation

Author for correspondence:
Bryne T. Ngwenya
e-mail: bryne.ngwenya@ed.ac.uk

Royal Society Publishing

Self-preservation strategies during bacterial biomineralization with reference to hydrozincite and implications for fossilization of bacteria

Bryne T. Ngwenya[1], Marisa Magennis[1], Francesca Podda[3] and Andrei Gromov[2]

[1]School of GeoSciences, and [2]School of Chemistry, University of Edinburgh, West Mains Road, Edinburgh EH9 3JW, UK
[3]Department of Chemical and Geological Sciences, University of Cagliari, Via Trentino 51, 09127 Cagliari, Italy

The induction of mineralization by microbes has been widely demonstrated but whether induced biomineralization leads to distinct morphologies indicative of microbial involvement remains an open question. For calcium carbonate, evidence suggests that microbial induction enhances sphere formation, but the mechanisms involved and the role of microbial surfaces are unknown. Here, we describe hydrozincite biominerals from Sardinia, Italy, which apparently start life as smooth globules on cyanobacterial filaments, and evolve to spheroidal aggregates consisting of nanoplates. Complementary laboratory experiments suggest that organic compounds are critical to produce this morphology, possibly by inducing aggregation of nanoscopic crystals or nucleation within organic globules produced by metabolizing cells. These observations suggest that production of extracellular polymeric substances by microbes may constitute an effective mechanism to enhance formation of porous spheroids that minimize cell entombment while also maintaining metabolite exchange. However, the high porosity arising from aggregation-based crystal growth probably facilitates rapid oxidation of entombed cells, reducing their potential to be fossilized.

1. Introduction

Annually in spring/summer, a cyanobacterial bloom triggers the precipitation of hydrozincite ($Zn_5(CO_3)_2(OH)_6$) along a small stream draining Pb–Zn mine wastes in southwest Sardinia, Italy (figure 1). Hydrozincite precipitation is due to photosynthetic alkalinization of the cyanobacterial cell surface [1,2] and probably serves to detoxify dissolved Zn, resulting in a polished discharge into the Mediterranean [1]. However, the precipitate also encrusts cells, which in the wider context of most microbes and particularly bacteria could potentially lead to death and entombment.

However, there is accumulating experimental evidence that induced biomineralization leads to specific morphologies that help prevent cell entombment. Aloisi *et al*. [3] showed that metabolizing cells of *Desulfovibrio lacustre* produce cell-bound organic nanoglobules that act as nucleation sites for calcium carbonate, which are subsequently released from the cell surface. Similarly, dolomite nucleation occurred in nanoglobules produced by the halophiles *Halomonas meridiana* and *Virgibacillus marismortui* [4]. In both the cases, production of these globules was seen as a mechanism to avoid self-entombment of the bacterial cell.

In nature, microbial cells occur mostly as biofilms embedded within an organic matrix of extracellular polymeric substances (EPS), consisting mostly of polysaccharides and proteins (amino acids) with lesser amounts of uronic and nucleic acids [5]. Experimental evidence suggests that EPS and other organic molecules enhance sphere formation during microbial induction of calcium carbonate precipitation [6,7]. These observations led us to hypothesize that organic secretions by microbes may constitute a global strategy to facilitate the development of

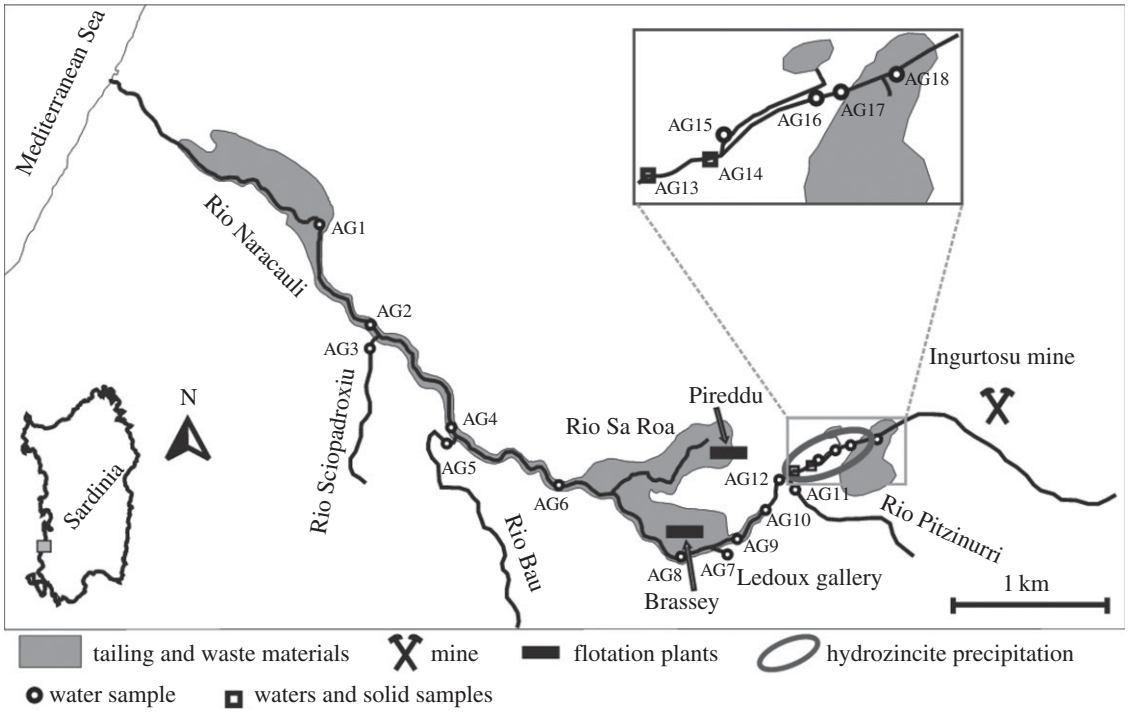

Figure 1. Map showing location of the Rio Naracauli in southwest Sardinia and sampling locations for hydrozincite bio-precipitates shown in figure 2.

spherical precipitates to avoid self-entombment. We used a combination of microscopic and spectroscopic observations supported by theoretical arguments to test this hypothesis.

2. Material and methods

We collected hydrozincite bio-precipitates from the Rio Naracauli in Sardinia (figure 1) in May 2006 and studied their mineralogy, morphology and textures using X-ray diffraction (XRD), scanning electron microscopy (SEM) and vibrational spectroscopy. To test the hypothesis that organic compounds are deployed by cells to control precipitate morphology, we also conducted abiotic hydrozincite precipitation experiments in which several L-amino acids (L-aspartic acid, L-glutamic acid and L-cysteine) and the model polysaccharide xanthan were used as surrogate components of microbial EPS [6].

Experiments were conducted in triple-neck, round-bottomed 250 ml flasks (Quickfit) containing 100 ml of an autoclaved equimolar solution (20 mM) of $ZnSO_4$ and $NaHCO_3$, and connected to a second flask containing approximately 10 g of $(NH_4)_2CO_3$. All additives were added to a final concentration of 1 mg ml^{-1} (except xanthan, 0.25 mg ml^{-1}) and mixed alongside controls without organic additives. The pH was monitored during mixing of the two solutions and adjusted to approximately pH 6 using concentrated HNO_3 (15.5 M, Merck Analar grade) in order to prevent precipitation during mixing [8]. The pH of the solution was monitored via an 8-channel meter (except for the control where pH was recorded manually since we did not have enough electrodes that fitted the 8-channel meter) by electrodes calibrated against Merck buffers (pH 4 and 7) inserted in the middle port of the flask and sealed against a rubber bung. Precipitation products were also examined using XRD, SEM and vibrational spectroscopy (attenuated total reflectance Fourier transform infrared (ATR-FTIR) and Raman), the latter referenced against a commercial hydrozincite standard (zinc carbonate basic) from Fluka.

XRD analysis was carried out on a Bruker D8 Advance diffractometer using CuKα primary radiation generated at an accelerating voltage of 40 kV. Samples were scanned in a range of 4–60° 2θ with a dwell time of 1 s/0.01 2θ, and diffracted X-rays were recorded by a Sol-x energy dispersive detector. SEM samples were mounted onto Al stubs covered in conductive (carbon) sticky discs and gold sputter-coated to a thickness of approximately 20 nm. A Philips XL30CP SEM with tungsten filament was used for field samples, with accelerating voltage of 20 kV, whereas additional SEM imaging for precipitates with organic additives was carried out using a CarlZeiss Sigma HDVP microscope at an accelerating voltage of 5 kV.

FTIR spectra were collected using a Bruker Vertex 70 spectrometer on a single bounce, Platinum ATR accessory fitted with a diamond crystal. Samples were finely ground using an agate pestle and mortar and a few milligrams were trapped under the diamond crystal. Absorbance was measured using a room temperature DLaTGS detector and spectra were collected and processed (including background subtraction) using OPUS v. 7.0 software.

Raman measurements were performed on an Ocean Optics QE65Pro Raman fiber optics spectrometer using a diode laser with excitation wavelength of 785 nm. All spectra were measured at laser power of 500 mW using a laser spot size of 100 µm. Data were collected in the spectral range 100–2815 cm^{-1}. Scan times were 1 s, and depending on the signal output 5–10 accumulations were collected in order to get reasonable signal-to-noise ratio. For asp-lab and glu-lab and xanthan gum samples, the spectra exhibited fluorescence, i.e. high level of background which masked the spectral features of the material. Therefore, these spectra were processed using the baseline subtraction procedure with cubic spline interpolation algorithm using Renishaw WiRE2 software.

3. Results

3.1. Structure of natural hydrozincite bio-precipitates

SEM was used on natural hydrozincite to establish its textural/spatial relationships to microbial cells and to investigate the mechanism of bio-precipitation. The hydrozincite displays a characteristic morphology consisting of botryoidal masses with a porous texture (figure 2*a*). As shown in previous studies [1,2,9], the spherical precipitates adhere to the bacterial sheath and are also associated with a meshwork of EPS (figure 2*b*), clearly demonstrating their biological origin. At high magnification, each sphere is made up of numerous nanoplates/

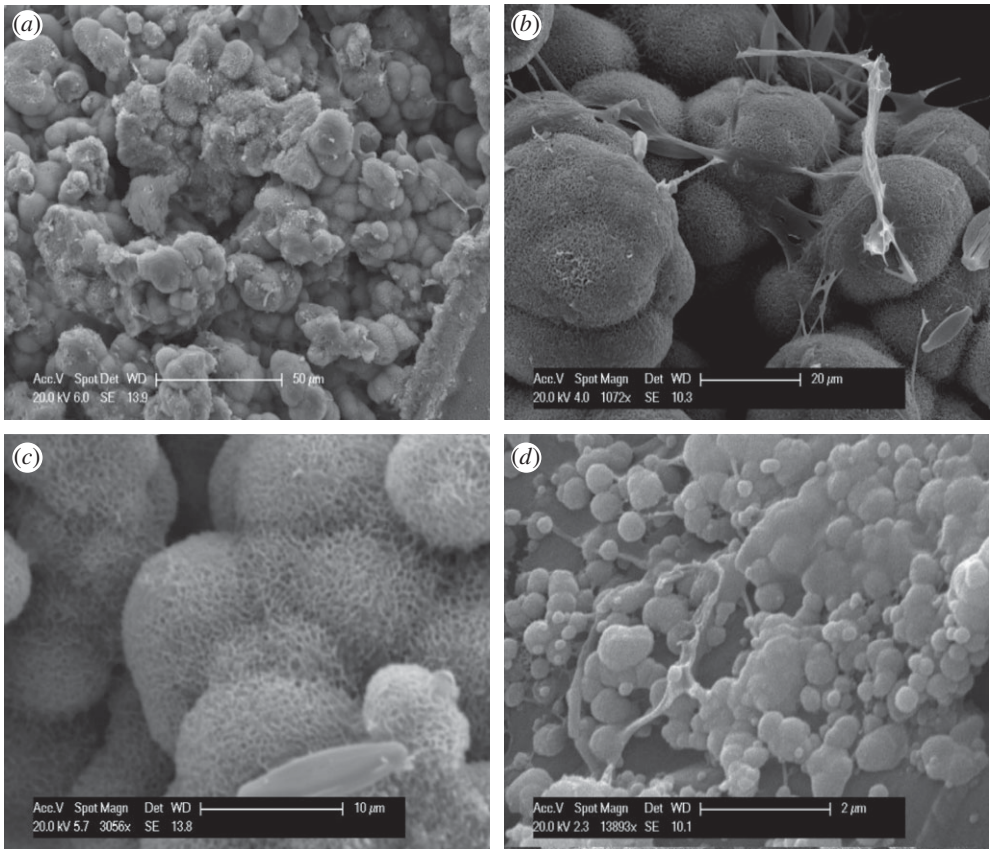

Figure 2. SEM photographs illustrating dominant morphologies and textures in hydrozincite bio-precipitates from Rio Naracauli. (*a*) General appearance of the bio-precipitates displaying botryoidal structure, (*b*) higher magnification of spheroids showing close association with organic strands thought to be EPS, (*c*) close-up view of the spheroids consisting of platy/needle-like aggregates and (*d*) even higher magnification image showing globular nature of early formed hydrozincite in association with EPS.

nanofibres with no specific orientation (figure 2*c*). Apparently, the growth of these spheres starts as smooth globules on/and surrounding the surface of the organic structures (figure 2*d*). These globules merge into each other as they grow and appear to maintain the smooth texture, with the porous structure only appearing at later stages of growth.

Similar textures/structures have been reported in the literature when other minerals precipitate in the presence of bacteria. Morin *et al.* [10] have described the mineral tooeleite ($Fe_6(AsO_3)_4(SO_4)(OH)_4{\cdot}4H_2O$) as exhibiting a reticulated structure consisting of nanosized platy crystallites, particularly when biologically catalysed. Furthermore, the mineral dypingite ($Mg_5(CO_3)_4(OH)_2.5H_2O$) was found to occur in the form of spherical aggregates consisting of platy crystals organized into rosettes [11]. The texture was most common in biotic experiments, although abiotic titrations of the water to high pH also produced rosettes. These observations offer circumstantial evidence that bacteria are involved in the development of the spherical aggregates, although it is unclear if the cell surface and/or exopolymeric substances are the critical variable. This prompted us to test the effect of organic additives on the structure of hydrozincite precipitates in abiotic experiments.

3.2. Effects of organic additives on hydrozincite structure

Based on the similarity of natural hydrozincite structures to structures described for other minerals and in experimental systems [3,7], we assumed that cells actively secrete globules (figure 2*d*) to serve as nucleation sites for hydrozincite. More specifically, we hypothesized that cells secrete organic compounds in the form of EPS that promote the formation of spherical aggregates as a probable strategy to avoid entombment [6]. This assumption was tested using experiments where 20 mM zinc sulfate solutions made to mimic the concentration in the Rio Naracauli were spiked with organic additives and incubated for just over one week. The experiments successfully precipitated hydrozincite, as confirmed by XRD analysis (data not shown). Control solutions without organic additives produced mostly flat discs (figure 3*a*,*b*). By contrast, solutions with organic additives produced precipitates consisting of a mixture of discs and irregular aggregates in proportions that appeared to depend on the additive. With L-aspartic acid, irregular aggregates dominate (figure 3*c*). At higher magnification, these aggregates display identical spheroidal aggregate morphology to the natural hydrozincite (figure 3*d*) and also contain very high porosity. As these experiments were sterile and abiotic, it is clear that this morphology arises only because of the presence of an organic additive. Addition of L-glutamic acid also produced a mixture of plates and aggregates in more or less equal proportions (figure 3*e*), with the aggregates also demonstrating botryoidal morphology similar to L-aspartic acid and natural samples (figure 3*f*). L-Cysteine produced mostly discs depicting 'tea-saucer' shapes but aggregates were also evident (figure 3*g*), although in this case with poorly developed botryoidal morphology (figure 3*h*). Finally, xanthan produced mostly irregular aggregates (figure 3*i*) which completely lacked botryoidal structure (figure 3*j*). Nevertheless, in the case of both L-cysteine and xanthan, the aggregates were also found to comprise nanoscopic plates similar to those

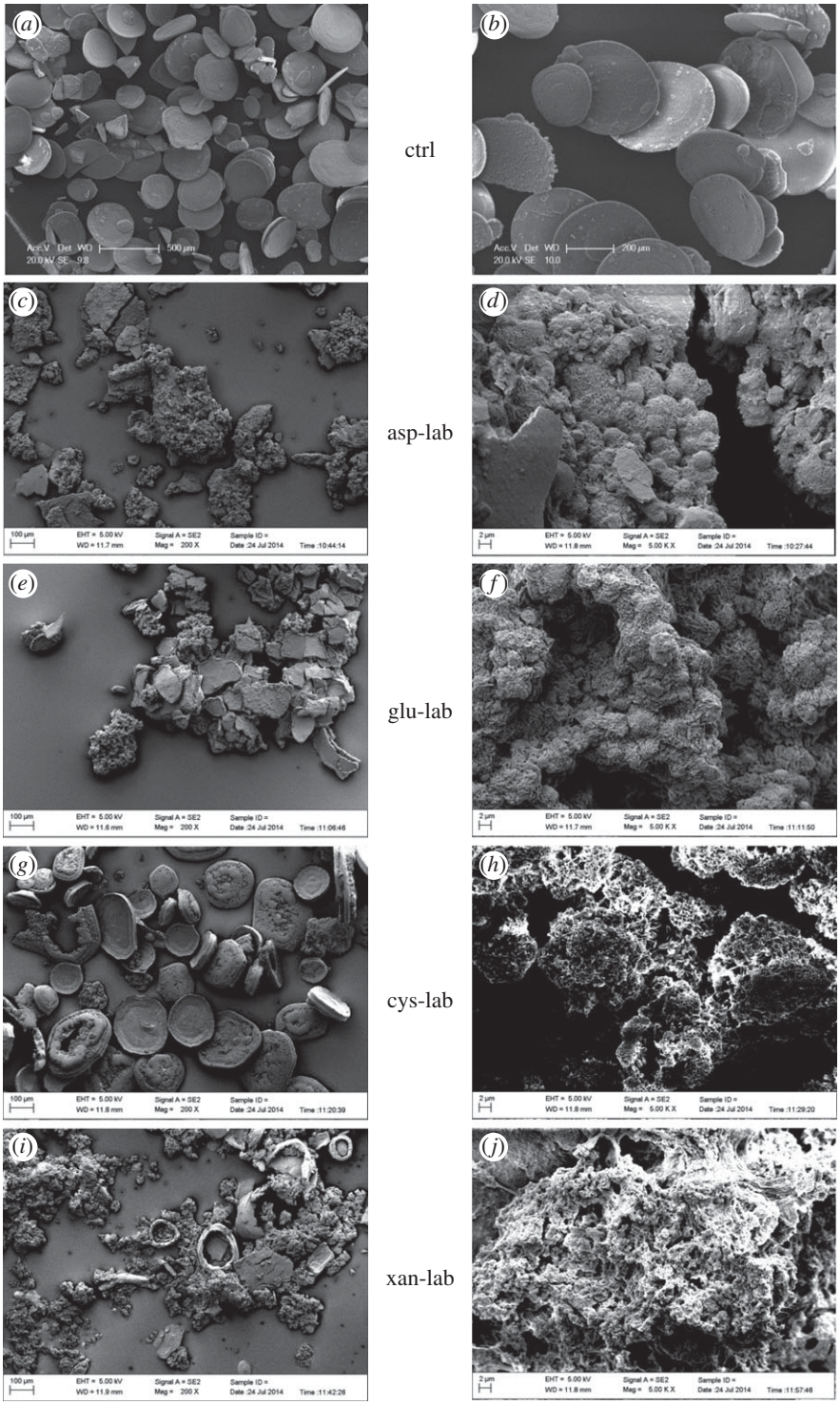

Figure 3. SEM photographs of hydrozincite precipitated under sterile conditions in the laboratory in (*a*,*b*) the absence of organic additives (ctrl) and (*c*–*j*) the presence of different organic additives (as labelled), simulating the presence of bacterial extracellular polymers. L-Aspartic acid (asp-lab), L-glutamic acid (glu-lab) and L-cysteine (cys-lab) were added to a concentration of 1 mg ml^{-1}, whereas xanthan (xan-lab) was added at 0.25 mg ml^{-1} to reduce suspension viscosity and facilitate precipitate recovery by filtration. Note the botryoidal structure similar to natural hydrozincite in the presence of L-aspartic and L-glutamic acids; this structure is poorly developed in precipitates with L-cysteine and xanthan.

forming the botryoidal aggregates in the presence of L-aspartic acid, L-glutamic acid and in natural hydrozincite.

3.3. Vibrational spectroscopy

As well as providing extra identification, vibrational spectroscopic analysis (ATR-FTIR and Raman) was conducted to probe the presence of organic additives in the synthetic precipitates, since such additives can often be incorporated during crystal growth [12]. ATR-FTIR data showed that all synthetic hydrozincites yielded spectra identical to both a commercial batch of zinc basic carbonate (Fluka) and the natural bio-precipitate from Rio Naracauri (figure 4*a*). Based on previous studies [13,14], the main frequencies within the recorded 400–3200 cm^{-1} range were due to symmetric stretching (1045 cm^{-1}), bending (837 cm^{-1}) and asymmetric stretching (1504 and 1388 cm^{-1}) modes of the CO_3^{2-} group. Only hydrozincite precipitated in the presence of L-cysteine displayed additional peaks at 1599 cm^{-1} (asymmetric bending), 1092 cm^{-1} (rocking), 997 cm^{-1} (rocking), 802 cm^{-1} (bending)

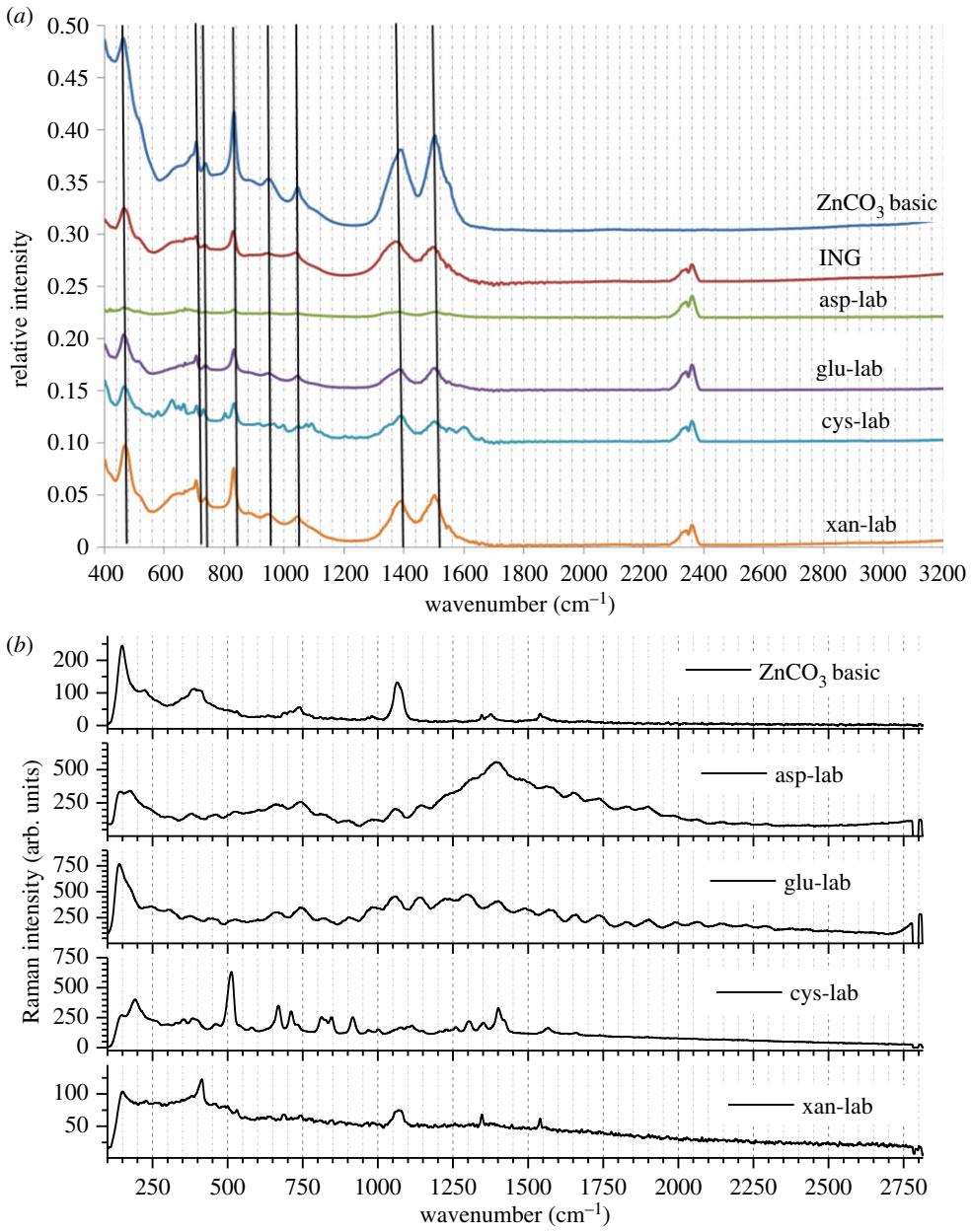

Figure 4. Infrared (*a*) and Raman (*b*) spectroscopic comparison of natural bio-precipitates (ING) and laboratory synthesized hydrozincites (asp-lab, glu-lab, cys-lab, xan-lab) with a commercial hydrozincite standard ($ZnCO_3$ basic). Note the slight red shift in the peaks at 1504 and 837 cm^{-1} in the presence of organic additives and for the natural sample in FTIR data, while both FTIR and Raman suggest possible incorporation of L-cysteine in the precipitate. The laboratory control without additives showed an identical spectrum to the commercial standard and is not shown. (Online version in colour.)

and 627 cm^{-1} (bending) modes. The first three are assigned to amine groups, whereas the latter two are due to CO_2^- based on comparison with Min'kov *et al.* [15]. Nevertheless, there appears to be a slight red shift in some of the peaks, most notably those at 1504 and 837 cm^{-1} in the presence of organic additives and for the natural sample.

Analysis by Raman spectroscopy confirmed the laboratory precipitates to be hydrozincite (figure 4) by comparison with characteristic peaks in a commercial hydrozincite standard and by the presence of peaks consistent with those from Frost & Hales [14]. Generally, peaks were weak and somewhat broad compared with the commercial standard (except for xanthan where peaks were relatively well defined). The presence of L-cysteine was also confirmed (figure 4*b*), with peaks in the region 500–950 cm^{-1} that are absent in the commercial hydrozincite. Meanwhile, there were no peaks that could be assigned to organic molecules in natural hydrozincite.

3.4. *In situ* measurements

Temporal trends in pH (figure 5) show that the gas diffusion approach using ammonium carbonate provides a good basis for simulating pH changes during microbial metabolism linked to urea metabolism [16,17]. Initially, the pH rises rapidly in the first 5 h followed by a period of nearly stable pH lasting up to 24 h. This stable pH period is associated with increasing turbidity of the solution (note that solutions containing L-aspartic acid and L-glutamic acid are clear at the initial pH of approximately 6 while those containing L-cysteine and xanthan start slightly cloudy). It is possible that this period constitutes the nucleation phase implying that hydrozincite precipitation is a proton-generating reaction that buffers pH increase due to ammonia for a while:

$$5Zn^{2+}_{(aq)} + 2(NH_4)_2CO_{3(g)} + 6H_2O_{(l)} \Leftrightarrow Zn_5(CO_3)_2(OH)_{6(s)} + 10H^+_{(aq)} + 4NH_{3(aq)}. \quad (3.1)$$

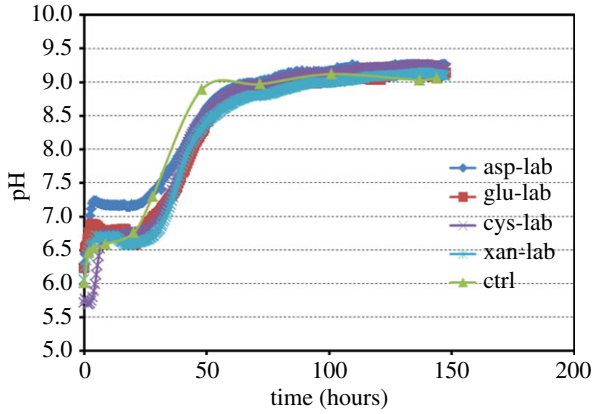

Figure 5. Graph showing changes in solution pH during laboratory experiments. The curves display similar trends consisting of a rapid increase in pH in the first 5 h, a nearly constant (buffered) region up to 25 h during which nucleation is thought to occur, and a third phase of rapid increase towards an asymptotic value around 9. Lines represent experiments containing L-aspartic acid (asp-lab), L-glutamic acid (glu-lab), L-cysteine (cys-lab), xanthan (xan-lab) and control without additives (ctrl). (Online version in colour.)

Subsequently, the pH rises rapidly again over the following 48 h towards an asymptotic value of approximately 9, probably associated with crystal growth and/or aggregation (see below).

4. Discussion

The main finding of this combined field and experimental study is that the induction of hydrozincite precipitation by cyanobacteria in the Rio Naracauri leads to specific morphologies which are only reproducible *in vitro* in the presence of organic additives. Clearly, of the two morphologies (discs and aggregates) produced in the experiments, spherical aggregates offer better scope for avoiding cell entombment. Sphere packing offers open channels (figure 6*a*) and potentially facilitates efficient exchange of nutrients as well as metabolic waste products. It follows that microbes would derive maximum benefit if they could facilitate the formation of spherical crystals. However, thermodynamic arguments indicate that the nucleation of a sphere is energetically less favourable than nucleation of discs/plates. To demonstrate this qualitatively, we compared free energy profiles for the heterogeneous formation of a critical stable nucleus for the two shapes shown in figure 6*a*,*b*. The relevant equations are [18,19] for a perfect sphere (which on a surface implies a wetting angle of 180°, see caption)

$$\Delta G_{\text{nucleus}} = 4\pi r^2\gamma - \frac{4\pi r^3 kT\ln S}{3v} \tag{4.1}$$

and for a circular disc [19]

$$\Delta G_{\text{nucleus}} = 2\pi rh\gamma - \frac{\pi r^2 hkT\ln S}{v}, \tag{4.2}$$

where r is the radius (m), γ is the surface free energy of the mineral (J m^{-2}), k is the Boltzmann constant, T is temperature (K), v is the molecular volume of the mineral (m^3), S is the relative saturation of the solution (dimensionless) and h is the height of a circular disc (m). The molecular volume of hydrozincite is about 2.2×10^{-28} m^3 (http://database.iem.ac.ru/mincryst/inf.php?hydrozin.cit) but a value for γ is not available in the literature. This deficiency need not preclude comparison of relative nucleation energies for the two shapes for a given surface free energy value. Using 0.6 J m^{-2}, which is in the lower range of surface free energies for carbonates [20], shows that a spherical critical nucleus has to overcome approximately 5 times more nucleation energy barrier than a disc-shaped nucleus (figure 6*c*) for the same solution saturation (SI ≈ 8) constrained by values measured in Rio Naracauli [9]. The critical radius, corresponding to the maximum in ΔG, is also larger for a sphere (22 nm) than a disc (11 nm), consistent with theoretical predictions [18]. Both outcomes are due to higher surface energy for generating a sphere. Although one cannot demonstrate that the final shape is that of the critical nucleus, these calculations imply that microbes must employ active strategies to facilitate formation of spherical aggregates from other crystal shapes.

One such strategy is the production of organic globules to act as nucleation sites for precipitation [3,4] (figure 2*d*). The exact mechanisms by which these organic globules catalyse carbonate nucleation are not known at present. While an alkaline environment necessary to produce HCO_3^- and CO_3^{2-} ions from the respired CO_2 can be generated through photosynthesis (cyanobacteria) and/or metabolic deamination of amino acids by heterotrophs [4,21], localized supersaturation of the carbonate can be achieved through complexation of the cation (Ca^{2+}, Mg^{2+}, Zn^{2+}) by functional groups on organic molecules/EPS in the globule. The bound cations then attract carbonate ions, effecting mineral precipitation [22]. In such a scenario, the shape of the final precipitate is determined by the globule and individual nuclei/crystals can grow in different shapes to lower crystallization energies. Cation binding probably also acts to lower saturation of the mineral [8], providing further protection from toxic metal ions. While the nature and composition of the organic molecules in nanoglobules have yet to be established and hence their ability to bind cations is unknown, bacterial EPS is known to effectively bind Ca^{2+} from solution [23].

Another mechanism by which organic molecules could promote spherical morphologies is through aggregation of non-spherical nanoscopic and microscopic crystals. Aggregation-based mineral growth [24] has been demonstrated in a number of studies in which organic molecules and polymers are present [25], leading to the formation of mesocrystals with oriented growth [24] or non-oriented crystal aggregates [12]. The accepted mechanism for such growth is that the interaction between organic molecules and crystal nuclei retards further growth of the nuclei, which hence occurs at a slower rate than aggregation [12]. Specifically, organic molecules might adsorb to different faces on crystal nuclei, leading to passivation of those faces. As demonstrated by a number of studies based on field and laboratory investigations [9–11,26] aggregate mineral structures are invariably present when precipitation occurs in the presence of bacteria, suggesting a common operative mechanism.

One outcome of growth by aggregation in the presence of organic additives is the possible incorporation of the organic molecules adsorbed on surfaces by trapping into the polycrystalline aggregate [12]. Hence, we subjected samples of natural and synthetic hydrozincite precipitates to vibrational spectroscopic analysis. Spectra of natural hydrozincite from the Rio Naracauli did not display peaks other than those present for commercial synthetic hydrozincite or experimental controls without additives. Given that cyanobacterial

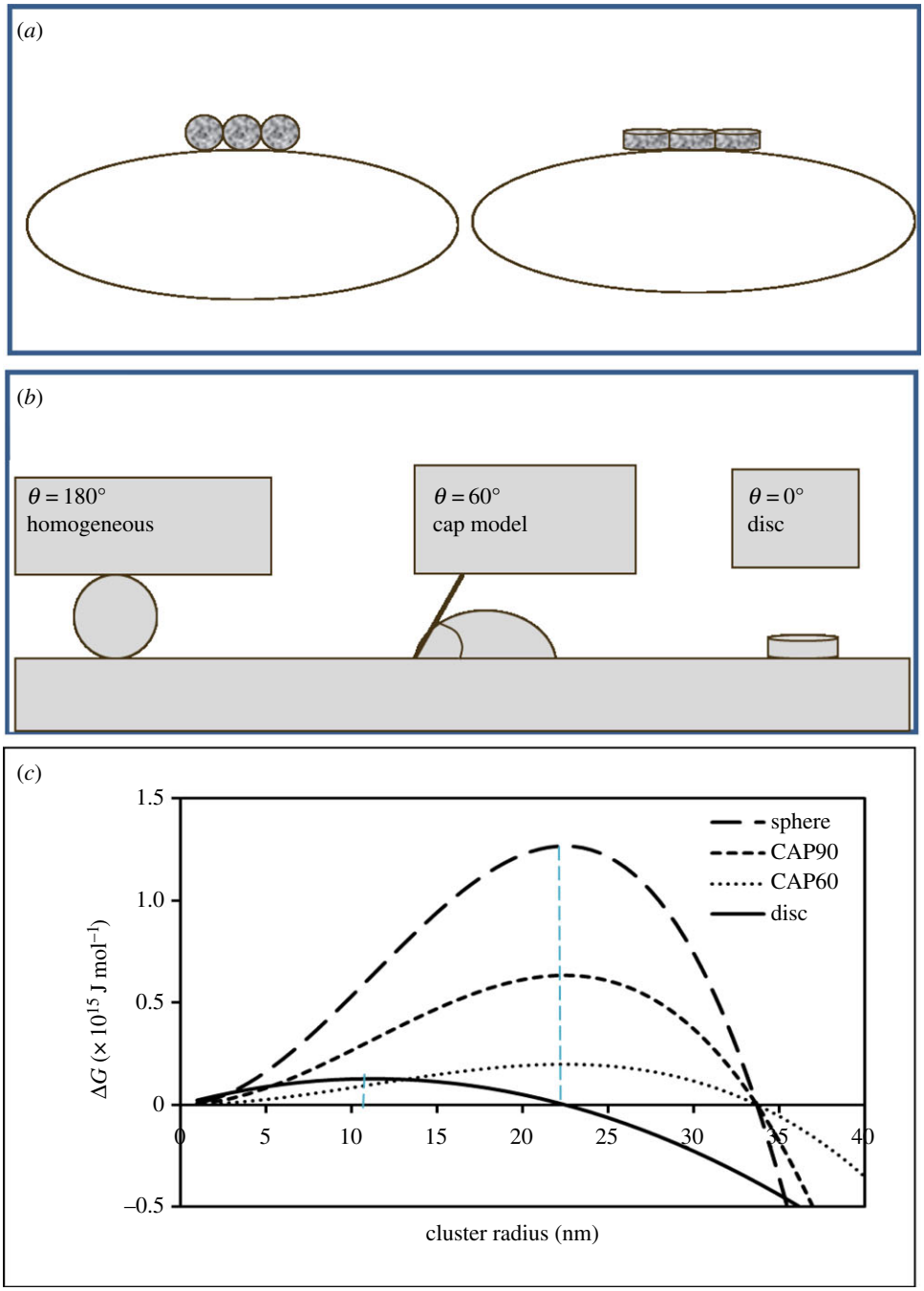

Figure 6. (*a*) Conceptual view of the relative likely potency to entomb a bacterial cell by spheres and discs and comparison of the thermodynamic drive for the nucleation of each shape (*b*,*c*), showing a lower energy cost of forming a disc-shaped nucleus. Note that equation (3.1) is multiplied by $(1 - \cos\theta)^2(2 + \cos\theta)/4$ for heterogeneous nucleation [18], where θ is the contact angle as shown in (*a*). Dotted vertical lines in (*c*) mark the maximum ΔG for the sphere and the disc and represent the radius of the critical cluster for each shape. (Online version in colour.)

filaments and strands of EPS are clearly present in these samples (figure 2*b*), this result is somewhat counterintuitive and may point to lack of sensitivity of the techniques used. Indeed, De Giudici *et al.* [2] demonstrated the incorporation of organic biopolymers using NMR spectroscopy. In the laboratory precipitates, distinct peaks were only present in hydrozincite precipitated in the presence of L-cysteine. While this may suggest that L-cysteine was incorporated into the synthetic hydrozincite, it is also possible that the vibrations are simply due to the presence of solid L-cysteine in the precipitate, since L-cysteine solutions were turbid even before hydrozincite precipitation commenced. However, xanthan was also insoluble under the starting conditions of the experiment and indeed had to be reduced significantly in concentration relative to other additives to facilitate filtration. On the other hand, there was a small but notable red shift in some peaks for samples with additives and in the natural sample (relative to the commercial standard), consistent with some structural modifications resulting from the presence of natural (EPS/cells) and artificial organic compounds.

5. Summary and wider implications

Our study has shown that the addition of organic additives mimicking EPS always appeared to induce aggregation, strongly suggesting that the differences in structure between control and organic spiked precipitates are due to the

presence of these additives (figure 2), and hence that the structures seen in natural samples may also be indicative of biological/organic control of the morphologies [2,10]. Lastly, we note that L-aspartic acid and L-glutamic acid induced the formation of botryoidal aggregates similar to those from Rio Naracauri, whereas L-cysteine and xanthan did not. These differences cannot be explained by observations from this study and must await further work; however, it is possible that they relate to the polarity and/or charge characteristics of the additives.

The significance of forming spherical aggregates becomes apparent when the precipitation of spherical grains is considered in the context of cell entombment by comparison with other precipitate morphologies. Since bacteria can only acquire nutrients and excrete metabolic by-products through their cell surfaces, maintaining an open pore network is critical to their survival in the face of adventitious mineral precipitation. We note that high porosities are also an inherent feature of microbial mat carbonates, tufa, thrombolites and stromatolites which are known to form in intimate association with EPS [27]. As schematically illustrated in figure 6*a*, spherical aggregates provide better scope for an open channel network compared to discs or other polycrystalline shapes. More importantly, the chaotic rather than oriented aggregate morphologies in both natural and synthetic samples with organic additives create additional pore network volume and connectivity, potentially affording nutrient/waste exchange despite apparent total entombment.

A potentially important consequence of porous aggregates precipitating on microbial surfaces is easy access to terminal electron acceptors for the oxidation of entombed cells when cells eventually die. As a result, preservation of cells is likely to be compromised, which may partly explain why we did not detect any organic material in natural samples (notwithstanding the visual presence of EPS by SEM, above). This will result in reduced propensity for fossilization of microbial cells in the geological record. In addition, such aggregates will be prone to compactive deformation and recrystallization to different shapes and crystal polymorphs. Lastly, we acknowledge that the botryoidal, nanoscopic morphology also occurs in otherwise organic-free and abiotic systems in nature. The consequence of these three factors is a somewhat compromised potential for the use of microbial biominerals as morphological biosignatures.

Acknowledgements. We thank Prof. Eleanor Campbell (Chemistry, Edinburgh) for access to the Raman spectrometer, Nicholas Odling (XRD) and Nicola Cayzer (SEM). We thank Tim Holt and Ruth Milne for editorial guidance and three anonymous reviewers for helping us to clarify our arguments.

Funding statement. This work was funded through a RCUK NERC grant (NE/C519462/1) with field support from the University of Cagliari approved by Prof. Luca Fanfani.

References

1. Podda F, Zuddas P, Minacci A, Pepi A, Baldi F. 2000 Heavy metal co-precipitation with hydrozincite [$Zn_5(CO_3)_2(OH)_6$] from mine waters caused by photosynthetic microorganisms. *Appl. Environ. Microbiol.* **66**, 5092–5098. (doi:10.1128/AEM.66.11.5092-5098.2000)
2. De Giudici G, Podda F, Sanna R, Musu E, Tombolini R, Cannas C, Musinu A, Casu M. 2009 Structural properties of biologically controlled hydrozincite: an HRTEM and NMR spectroscopic study. *Am. Mineral.* **94**, 1698–1706. (doi:10.2138/am.2009.3181)
3. Aloisi G, Gloter A, Krüger M, Wallmann K, Guyot F, Zuddas P. 2006 Nucleation of calcium carbonate on bacterial nanoglobules. *Geology* **34**, 1017–1020. (doi:10.1130/G22986A.1)
4. Sánchez-Román M, Vasconcelos C, Schmid T, Dittrich M, McKenzie JA, Zenobi R, Rivadeneyra MA. 2008 Aerobic microbial dolomite at the nanometer scale: implications for the geologic record. *Geology* **36**, 879–882. (doi:10.1130/G25013A.1)
5. Frolund B, Palmgren R, Keiding K, Nielsen PH. 1996 Extraction of extracellular polymers from activated sludge using a cation exchange resin. *Water Res.* **30**, 1749–1758. (doi:10.1016/0043-1354(95)00323-1)
6. Braissant O, Cailleau G, Dupraz C, Verrecchia EP. 2003 Bacterially-induced mineralization of calcium carbonate in terrestrial environments: the role of exopolysaccharides and amino acids. *J. Sedimentary Res.* **73**, 485–490. (doi:10.1306/111302730485)
7. Bontognali TRR, Vasconcelos C, Warthmann RJ, Dupraz C, Bernasconi SF, McKenzie JA. 2008 Microbes produce nanobacteria-like structures, avoiding cell entombment. *Geology* **36**, 663–666. (doi:10.1130/G24755A.1)
8. Tourney J, Ngwenya BT. 2009 Bacterial extracellular polymeric substances (EPS) mediate $CaCO_3$ morphology and polymorphism. *Chem. Geol.* **262**, 138–146. (doi:10.1016/j.chemgeo.2009.01.006)
9. Medas P, Cidu R, Lattanzi P, Podda F, Wanty RB, de Giudici G. 2012 Hydrozincite seasonal precipitation at Naracauli (Sardinia-Italy): hydrochemical factors and morphological features of the biomineralisation process. *Appl. Geochem.* **27**, 1814–1820. (doi:10.1016/j.apgeochem.2012.02.016)
10. Morin G, Juillot F, Casiot C, Bruneel O, Personne J-C, Elbaz-Poulichet F, Leblanc M, Ildefonse P, Calas G. 2003 Bacterial formation of tooeleite and mixed arsenic(III) or arsenic(V)-iron(III) gels in the Carnoules acid mine drainage, France. A XANES, XRD and SEM study. *Environ. Sci. Technol.* **37**, 1705–1712. (doi:10.1021/es025688p)
11. Power IM, Wilson SA, Thom JM, Dipple GM, Southam G. 2007 Biologically induced mineralization of dypingite by cyanobacteria from an alkaline wetland near Atlin, British Columbia, Canada. *Geochem. Trans.* **8**, 13. (doi:10.1186/1467-4866-8-13)
12. Kulak AN, Iddon P, Yuting LI, Armes SP, Colfen H, Paris O, Wilson RM, Meldrum FC. 2007 Continuous structural evolution of calcium carbonate particles: a unifying model of copolymer-mediated crystallization. *J. Am. Chem. Soc.* **129**, 3729–3736. (doi:10.1021/ja067422e)
13. Music S, Popovic S, Malijkovic M, Dragcevic D. 2002 Influence of synthesis procedure on the formation and properties of zinc oxide. *J. Alloys Compounds* **347**, 324–332. (doi:10.1016/S0925-8388(02)00792-2)
14. Frost R, Hales M. 2007 Synthesis and vibrational spectroscopic characterization of synthetic hydrozincite and smithsonite. *Polyhedron* **26**, 4955–4962. (doi:10.1016/j.poly.2007.07.002)
15. Min'kov VS, Chesalov YA, Boldyreva EV. 2008 Study of the temperature effect on IR spectra of crystalline amino acids, dipeptides, and polyamino acids. IV. L-cysteine and DL-cysteine. *J. Struct. Chem.* **49**, 1022–1034. (doi:10.1007/s10947-008-0174-5)
16. Tobler DJ, Cuthbert MO, Greswell RB, Riley MS, Renshaw JC, Handley-Sidhu S, Phoenix VR. 2011 Comparison of rates of ureolysis between *Sporosarcina pasteurii* and an indigenous groundwater community under conditions required to precipitate large volumes of calcite. *Geochim. Cosmochim. Acta* **75**, 3290–3301. (doi:10.1016/j.gca.2011.03.023)
17. Martin D, Dodds K, Ngwenya BT, Butler IB, Elphick SC. 2012 Inhibition of *Sporosarcina pasteurii* under anoxic conditions: implications for subsurface carbonate precipitation and remediation via ureolysis. *Environ. Sci. Technol.* **46**, 8351–8355. (doi:10.1021/es3015875)
18. Mullin JW. 2001 *Crystallisation*, p. 600. London, UK: Butterworth-Heinemann.
19. Markov IV. 2003 *Crystal growth for beginners: fundamentals of nucleation, crystal growth and epitaxy*, p. 546. London, UK: World Scientific.

20. De Leeuw NH, Parker SC. 1998 Surface structure and morphology of calcium carbonate polymorphs calcite, aragonite and vaterite: an atomistic approach. *J. Phys. Chem. B* **102**, 2914–2922. (doi:10.1021/jp973210f)
21. Ngwenya BT. 2007 Enhanced adsorption of zinc is associated with aging and lysis of bacterial cells in batch incubations. *Chemosphere* **67**, 1982–1992. (doi:10.1016/j.chemosphere.2006.11.050)
22. Braissant O, Decho AW, Przekop KM, Gallagher KL, Glunk C, Dupraz C, Visscher PT. 2009 Characteristics and turnover of exopolymeric substances in a hypersaline microbial mat. *FEMS Microbiol. Ecol.* **67**, 293–307. (doi:10.1111/j.1574-6941.2008.00614.x)
23. Braissant O, Decho AW, Dupraz C, Glunk C, Perzekop KM, Visscher PT. 2007 Exopolymeric substances of sulfate-reducing bacteria: interactions with calcium at alkaline pH and implication for formation of carbonate minerals. *Geobiology* **5**, 401–411. (doi:10.1111/j.1472-4669.2007.00117.x)
24. Banfield JF, Welch SA, Zhang H, Ebert TT, Penn RL. 2000 Aggregation-based crystal growth and microstructure development in natural iron oxyhydroxide biomineralization products. *Science* **289**, 751–754. (doi:10.1126/science.289.5480.751)
25. Hua T, Wentao M, Leilei W, Peng W, Jiming H, Lianxin C. 2004 Control over the crystal phase, shape, size and aggregation of calcium carbonate via a L-aspartic acid inducing process. *Biomaterials* **25**, 3923–3929. (doi:10.1016/j.biomaterials.2003.10.038)
26. Long C, Yuhua S, Anjian X, Bei H, Rong J, Ruiyong G, Wenzhong T. 2009 Bacteria-mediated synthesis of metal carbonate minerals with unusual morphologies and structures. *Crystal Growth Des.* **9**, 743–754. (doi:10.1021/cg800224s)
27. Josef PJ, Arp G, Reitner J. 2008 Kalkowsky's type stromatolites and other microbialites of Lower Saxony. In *Geobiology of stromatolites. International Kalkowsky Symposium—abstract volume and field guide to excursions* (eds J Reitner, N-V Quéric, M Reich), pp. 141–202. Göttingen, Germany: Universitätsverlag Göttingen.